

## Chapter

# Effect of ECAE Die Angle on Microstructure Mechanical Properties and Corrosion Behavior of AZ80/91 Magnesium Alloys

*Gajanan Manjunath Naik, Sachin Bandadka,  
Manjaiah Mallaiah, Ravindra Ishwar Badiger  
and Narendranath Sannayellappa*

## Abstract

Magnesium alloys have poor tensile strength, ductility and corrosion resistance properties associated with other engineering materials like aluminum alloys, steels and superalloys etc. Therefore, many researchers worked on equal channel angular pressing of magnesium alloys to improve the mechanical properties and corrosion resistance. In this work, the effect of channel angles on material properties was investigated during equal channel angular pressing of AZ80/91 magnesium alloy using processing route-R at 598 K processing temperature. Channel angles of  $90^{\circ}$  and  $110^{\circ}$ , common corner angle of  $30^{\circ}$  have been considered for the study. It has been revealed that the channel angle has a significant influence on deformation homogeneity, microhardness, ultimate tensile strength, ductility, and corrosion behavior of AZ80/91 magnesium alloys. Specifically, AZ80/91 Mg alloys processed through  $90^{\circ}$  channel angle i.e. die A is considered as optimal die parameter to improve above-said material properties. Investigation showing concerning as-received AZ80 and AZ91 Mg alloy indicates 11%, 14% improvement of UTS and 69%, 59% enhancement in ductility after processing through 4P through die A ( $90^{\circ}$ ) at 598 K respectively. Also, the corrosion rate reduces to 97% and 99% after processing the sample with 4P-ECAP die A ( $90^{\circ}$ ) at the same processing temperature for AZ80 and AZ91 Mg alloys respectively. This is mainly due to grain refinement and distribution of  $Mg_{17}Al_{12}$  secondary phase during ECAP.

**Keywords:** ECAP, magnesium alloys, microstructure, mechanical properties, corrosion resistance

## 1. Introduction

Wrought magnesium alloys are one of the most promising lightweight materials of special interests in structural applications due to their homogeneous microstructure and improved mechanical properties compared to as-cast Mg alloys [1]. Mg alloys are one of the most reactive metals that have poor corrosion resistance and low mechanical properties, which limit its applications in industries. Therefore

enhancement of mechanical properties and corrosion resistance has led to greater interest in magnesium alloys because of its special applications [2–4]. Presently much effort is required for preparation of magnesium alloys with a grain size lower than 1  $\mu\text{m}$ , i.e. ultrafine-grained (UFG) materials to improve the strength and corrosion resistance of Mg alloys, many researchers worked and finally developed a severe plastic deformation (SPD) process which greatly contributes towards grain refinement and distribution of secondary phases to enhance mechanical and corrosion properties [5]. However, in SPD, ECAP is most developed and frequently used metal-working technique for significant materials hardening due to increasing dislocation density and considerable grain size reduction to sub-micro-level [6]. Finally, ultrafine grain structure and uniformly distributed secondary phase particles increase re-passivation tendency, which exhibits the improved mechanical properties and corrosion resistance. The ECAP process was planned with two equal channels: traversing at particular angles called the die channel angle ( $\phi$ ) and the corner angle ( $\psi$ ) subtended at the channels' intersection. In this work, the effect of ECAP die channel angles and processing temperature on microstructures, mechanical properties and corrosion resistance of ECAPed AZ80/91 Mg alloys were investigated.

## 2. Experimental work

### 2.1 Wrought AZ80/91 series magnesium alloys

Wrought AZ80 and AZ91 commercially available magnesium-based alloy, was selected as a workpiece material because of its high strength and low cost when compared to other magnesium-based alloys. The Mg alloy was procured in the form of a rod with dimensions 18 mm diameter and 200 mm length, from Exclusive Magnesium Pvt. Limited, Hyderabad, India. The chemical composition of AZ80/91 Mg alloys. Also, chemical composition presented along with the microstructure shown in **Figures 1** and **2**.

### 2.2 Equal channel angular extrusion

Die-Material: Hot Die steel (HDS) was used for die making. The ECAE die design was done by using solid edge V.7 software and fabrication was carried out at Government Tool Room and Training Centre (GTTC) Baikampady, Mangalore, Karnataka, India. **Figure 3** depicts the ECAE die having  $90^\circ$  and  $110^\circ$  channel angle

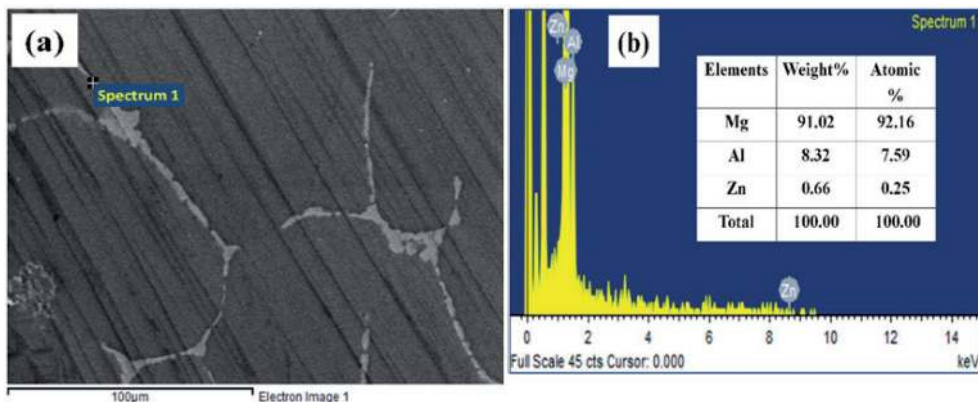


**Figure 1.**  
AZ80 Mg alloy (a) microstructure (b) EDS results.

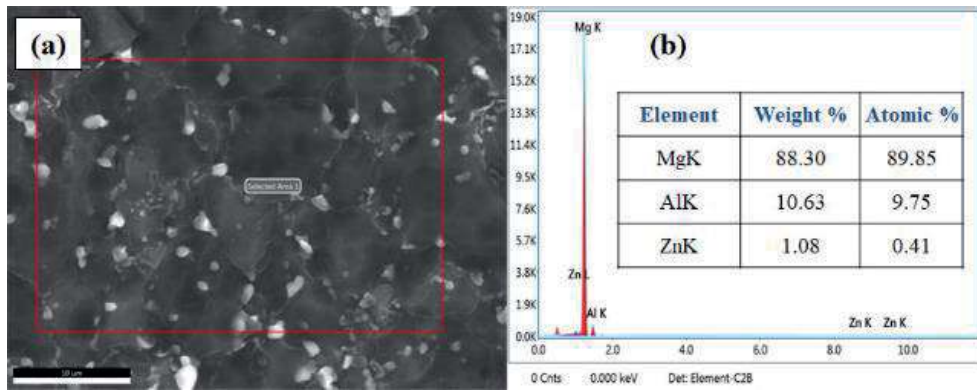


**Figure 2.**  
 AZ91 Mg alloy (a) microstructure (b) EDS results.

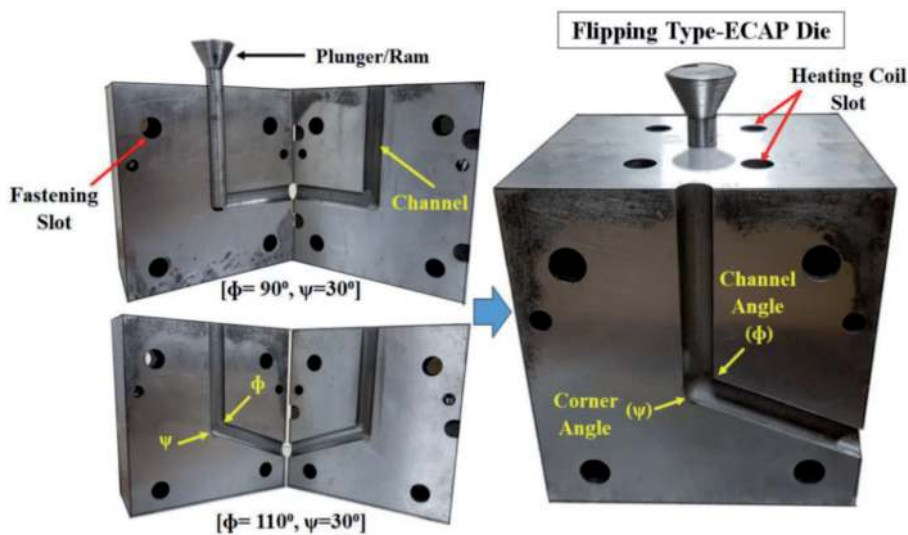


**Figure 3.**  
 ECAP die having 90° and 110° channel angle and 30° corner angle (Naik et al. Copyrights: Diary number: 14668/2018-CO/L., Reg. No: L-79923/2018).

and 30° corner angle. An equal channel angular extrusion thermo-mechanical apparatus is provided grain refinement to improve mechanical properties and corrosion resistance of magnesium alloys. ECAE is promising extrusion technique to achieve ultra-fine equiaxed grains without changing the shape of the workpiece. The extrusion die assembly having two angles such as channel angle ( $\phi$ ) and corner angle ( $\psi$ ) which decides the induced shear strain during ECAP. Current study focusses on the effect of ECAE die angles on microstructure, mechanical properties and corrosion resistance of AZ80/91 Mg alloys. In the present study route, *R* was considered to deform the material to achieve a fine grain structure. Route *R*: the specimen is inverted to the original position in each ECAP passes. The experimental setup of equal channel angular extrusion is shown in **Figure 4**. During operation ECAP die (**Figure 4**) is placed on the base plate of UTM and plunger is aligned exactly to the center of die where the specimen is placed inside the channel for pressing. The sample is placed in the die channel and needs to make sure that the temperature of the specimen also reached the 598 K.

A lubricant as Molybdenum disulfide ( $\text{MoS}_2$ ) was used to minimize the frictional effects between samples and die. After attaining the required

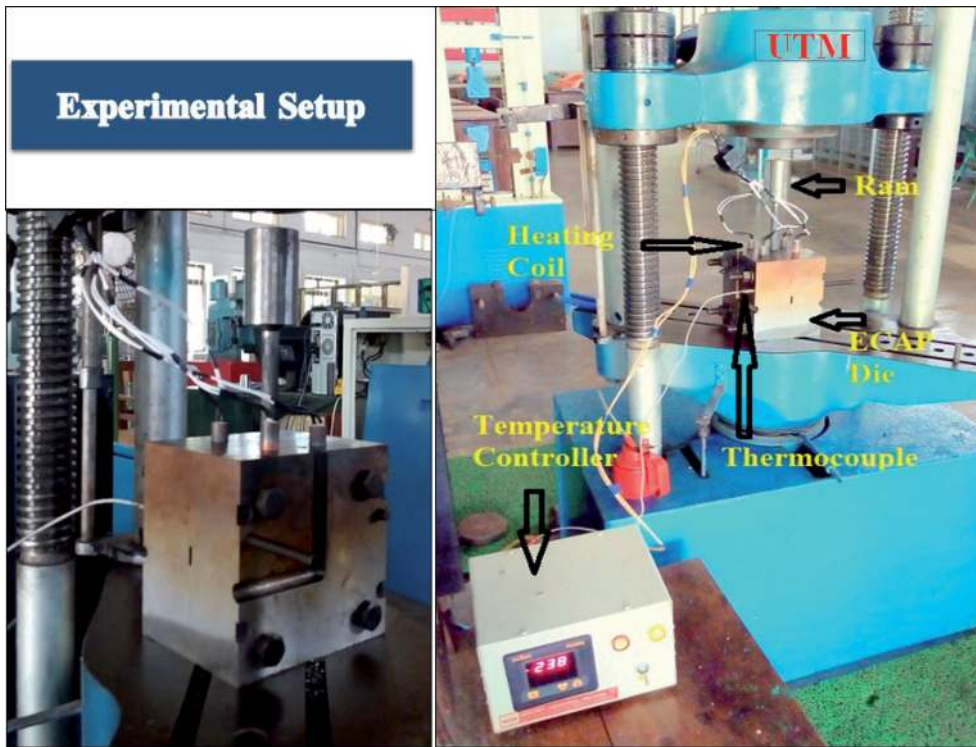


**Figure 4.**  
*Equal channel angular extrusion experimental setup.*

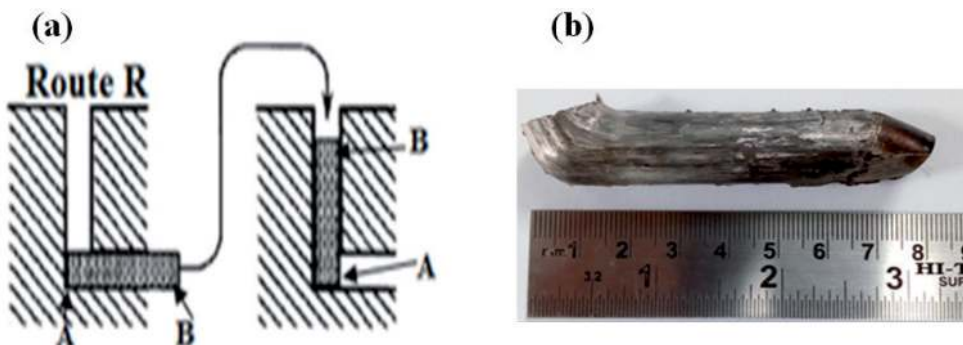


**Figure 5.**  
*(a) Route-R and (b) ECAPed sample.*

temperature, the sample is pressed by applying a load at the rate of 1 mm/sec ram speed using plunger attached to the UTM for deformation of the specimen. The channels are intersected to impose the total strain on the material to get a fine grain structure. This process is repeated by using route R, where the samples were inverted from its initial position between two successive passes as shown in **Figure 5(a)**. The processed samples after ECAP operation is shown in **Figure 5(b)** [7–12].

### 2.3 Microstructural characterization

This section focuses on all characterization techniques of ECAPed magnesium alloys including all forms of microscopy and analysis especially microanalysis and surface analytical techniques. The methodology of microstructure analysis and phase identification are also discussed.

### 2.3.1 Optical microscope

Specimens for microstructure inspection were prepared by mechanical polishing with silicon carbide abrasive papers (grades of 400, 800, 1000, 1200, 1500, 2000) followed by cloth polishing using diamond paste and kerosene for obtaining mirror finish surface and finally cleaned with acetone. Further, Etching was carried on the polished surface for approximately 3 to 5 s, in a solution of 4.2 g picric acid, 10 ml acetic acid, 10 ml distilled water and 70 ml ethanol for 3–5 s [8–12]. So that sample turns light brown and washed with running distilled water and dried. Microstructures and elements distributions were observed and analyzed using optical microscopy by image analyzer facilitated BIOVIS material plus software, and average grain sizes were measured by linear intercepts method according to ASTM E-112. Same samples were observed under a scanning electron microscope.

### 2.3.2 Scanning electron microscopy

Scanning electron microscope (SEM) equipped with energy dispersive spectroscopy (EDS) Backscattered electron (BSE) detector coupled with the EDS allows for composition identification of materials. Scanning Electron Microscopy Model: JEOL JSM–6380LA from JEOL, USA, operated at 30 kV; Magnification range–3,00,000 $\times$ , which allows studying the microstructures and surface morphologies.

### 2.3.3 X-Ray diffraction

X-ray diffraction (XRD) is one of the primary techniques used for the characterization of crystalline solids and determination of their structure or phases. XRD measurements are carried out in M/s Proto Manufacturing Ltd., CANADA make PROTO–iXRD MGR40, wherein the analysis was carried out  $2\theta$ : an angular range of  $20^\circ$  to  $90^\circ$  at a scanning speed of  $2^\circ/\text{min}$ . The XRD patterns obtained were analyzed with the help of PCPDFWIN software to identify the formation of primary, secondary and ternary phases.

## 2.4 Mechanical testing

### 2.4.1 Microhardness test

Microhardness test is also performed on as-received heat-treated and some of the deformed or ECAPed samples. The measurements were carried out at a load of 100gm and dwell of 13 s the microhardness was calculated using the expression [13]. Microhardness Model: MVH–S–AUTO from OMNI TECH, PUNE, INDIA.

### 2.4.2 Tensile test

The tensile test is used to evaluate the strength and ductility of as-received and equal channel angular extruded sample. Specimens were prepared according to the ASTM-E8 standard with 16 mm gauge length. The tensile properties of magnesium alloys were measured using UTM-Shimadzu AG-X plus™ equipped with 100 kN load cell and operated with a steady cross-head speed of 0.25 mm/min during all the tensile tests. Three samples were tested for each condition and uniaxial tensile testing was accomplished at room temperature and average reading was calculated and presented.

## 2.5 Electrochemical corrosion test

Corrosion study of AZ80/91 wrought Mg alloys was investigated using electrochemical corrosion analyzer, model: Gill AC-1684, supplied by Tech-science Pvt. Limited, Pune (India). The potentiodynamic polarization tests were conducted in 3.5 wt.% NaCl solution to estimate corrosion resistance or rate of corrosion of AZ80/91 wrought alloys. The auxiliary electrode (AE) was made of graphite (Gr) and the reference electrode (RE) was made of a saturated calomel electrode (SCE). 1cm<sup>2</sup> area of the working electrode (AZ80/91 alloys) was exposed to the 3.5 wt.% NaCl solution. Before the electrochemical corrosion test, specimens were polished with 600, 800, 1000, 1200, 1500, 2000 grit emery papers and washed with ethanol. The specimens were kept in corrosion cell kit in NaCl solution for 20 min to stabilize the open circuit potential (OCP). Further, the AC impedance test of starting frequency 10 kHz and ending frequency 10 MHz with a scan speed of 5 mV/s and cyclic sweep experiments with -250 to +250 mV was carried on the electrochemical analyzer. Surface morphology of the corroded samples was examined by SEM. The corrosion product was removed using 200 g/L of chromic acid and 10 g/L of AgNO<sub>3</sub> solutions. The corrosion rate of the alloy was calculated by using Eq. (1).

$$CR (\text{mm / y}) = 3.27 \times 10^{-3} \frac{i_{\text{corr}} X A}{\rho} \quad (1)$$

where CR is the corrosion rate in miles per year, A is the molar mass (for magnesium 24.3 g/mol),  $I_{\text{corr}}$  is the corrosion current density in  $\mu\text{A}/\text{cm}^2$ , n is the valance and  $\rho$  is the density ( $1.74 \text{ g}/\text{cm}^3$ ).

## 3. Results and discussion

### 3.1 Effect of ECAP die channel angle on AZ80/91 magnesium alloy

So far, many simulation studies have been executed to examine the impact of different die parameters on deformation homogeneity, strain rate, workflow etc. Although many researchers have been carried out on the efficiency of ECAP process routes and influences of various ECAP parameters on the strain behavior [14], there is limited work on a study of the effect of channel angle on grain size and other material properties through experimentally. In this chapter, the effect of ECAP channel angle on grain size, microhardness, tensile behavior and corrosion rate for different passes were analyzed using working temperatures of 598 K Furthermore, die A was used for examining above said material properties since this die gives the best results.

#### 3.1.1 Microstructure evolution of AZ80 Mg alloy

The optical microstructures of as-received, homogenized at 673 K-24 h sample and those after ECAP processed specimens are shown in **Figures 6** and 7. The microstructure of the as-received AZ80 Mg alloy presents the  $\alpha$ -Mg and  $\beta$ -Mg<sub>17</sub>Al<sub>12</sub> secondary phases along the grain boundaries indicated in **Figure 6(a)**. After homogenized at 673 K for 24 h secondary phases were partially dissolved along the grain boundaries as shown in **Figure 6(b)** this partial dissolution of secondary phases was achieved before ECAP and this sample is designated as OP specimen. **Figure 7** presents the optical images of the ECAPed AZ80 Mg alloy processed

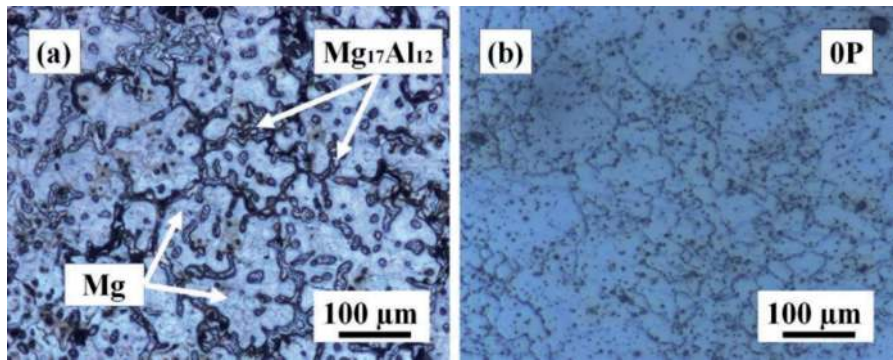


**Figure 6.**  
Optical images of (a) as-received (b) homogenized at 673 K-24 h.

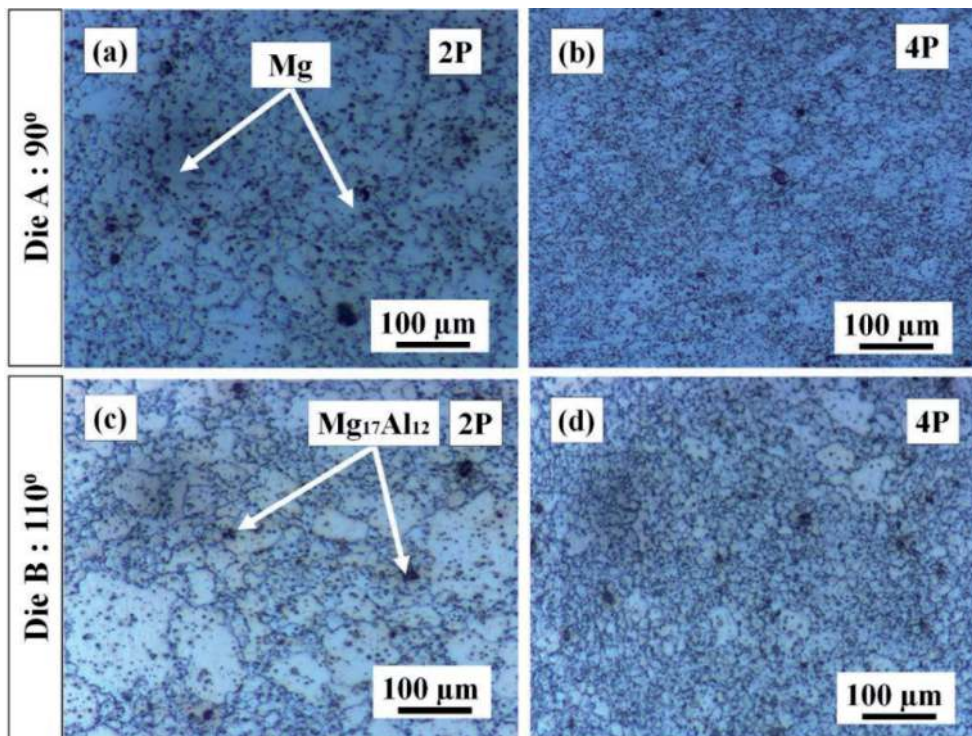


**Figure 7.**  
Optical images for die A: (a) 2P (b) 4P and die B: (c) 2P and (d) 4P ECAP passes.

through two ECAP die of 2 and 4 passes at 598 K processing temperature, in which the white and black contrast within the grains and along the grain boundaries represents  $\alpha$ -Mg primary phase and  $\beta$ -Mg<sub>17</sub>Al<sub>12</sub> secondary phases respectively. Also, the presence of  $\alpha$ -Mg and  $\beta$ -Mg<sub>17</sub>Al<sub>12</sub> phase in AZ80 alloys was confirmed through by the XRD analysis shown in **Figure 8**. The microstructure of the ECAPed Mg alloy showed significant grain refinement and bi-modal grains after ECAP of two passes for both die A and B, as shown in **Figure 7(a)** and **(c)**. These heterogeneous grains were typically obtained under the condition of lower deformation. When ECAP passes were gradually increased up to four passes bi-modal grain structure disappeared due to a large amount of induced plastic strain, as a result of the average grain size of ECAP-4P through die A was  $\sim 6.35 \mu\text{m}$  and the secondary phases are uniformly distributed throughout the material as shown in **Figure 7(b)**. Whereas ECAP-4P processed through die B exhibited slightly larger grains compared to

die A, the obtained grain size is of about  $\sim 9.77 \mu\text{m}$ . Hence, the effectiveness of grain refinement can be enhanced based on a channel angle, particularly, material processed through  $90^\circ$  channel angle exhibited better grain refinement.

### 3.1.2 Microstructure evolution of AZ91 Mg alloy

**Figure 9** shows the microstructure of the as-received and homogenized AZ91 Mg alloy. The microstructure of the as-received AZ91 Mg alloy shows a coarse  $\alpha$ -Mg phase and  $\beta$ - $\text{Mg}_{17}\text{Al}_{12}$  secondary phase along the grain boundaries which is confirmed through XRD analysis as shown in **Figure 8**.

The mean grain size of as-received Mg alloy is  $\sim 58.69 \mu\text{m}$  as shown in **Figure 9(a)**, measured by the linear intercept method (ASTM E 112). From **Figure 9(b)**, it could be found that after homogenization treatment at 673 K for 24 h the slight increase of mean grain size of Mg alloy of  $\sim 59.82 \mu\text{m}$  was observed this is due to grain growth

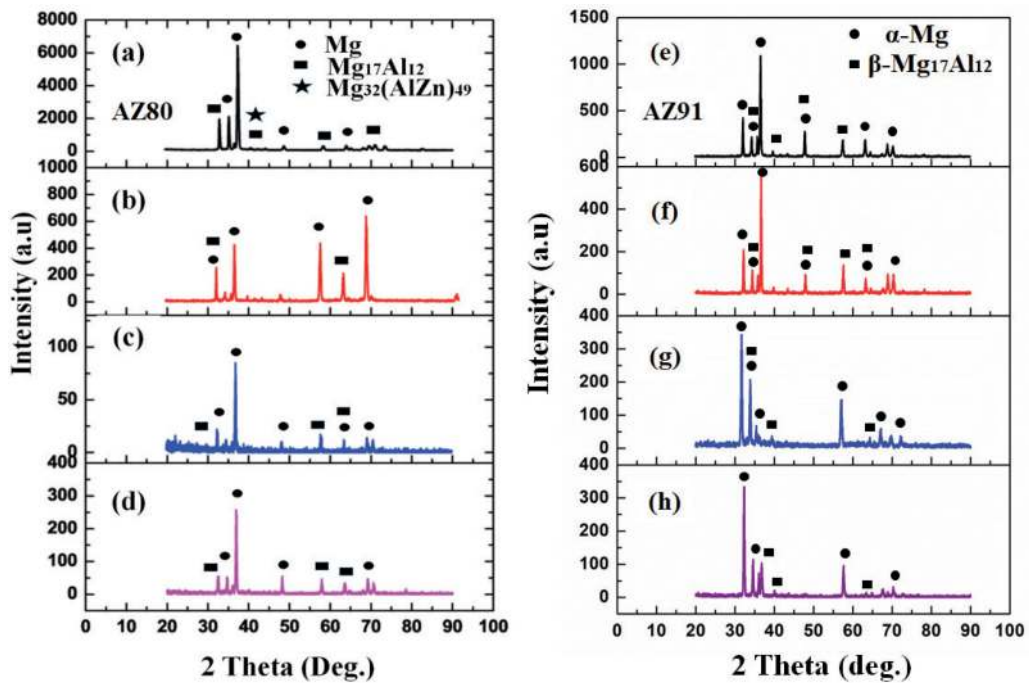


**Figure 8.** XRD analysis on AZ80 Mg alloys (a) as-received (b) homogenized at 673 K-24 h (c) die A: 2P at 598 K (d) die A: 4P at 598 K. XRD analysis on AZ91 Mg alloys (e) as-received (f) homogenized at 673 K-24 h (g) die A: 2P at 598 K and (h) die A: 4P at 598 K.

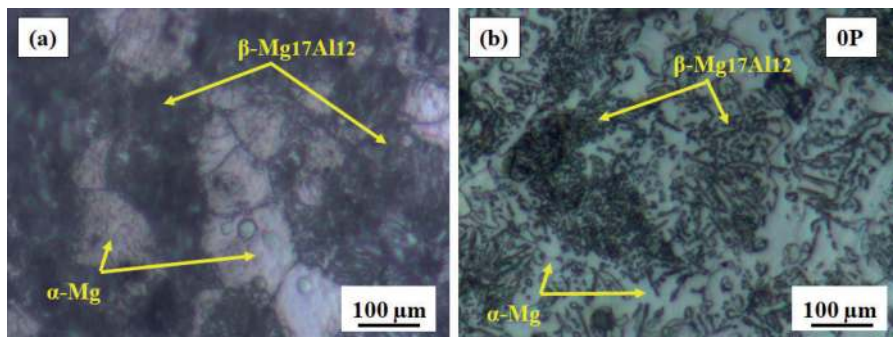


**Figure 9.** Optical images of (a) as-received (b) homogenized at 673 K-24 h.



effect during the homogenization process. Similar observations are made by Nikulin et al. [15]. After ECAP, the microstructure of the alloy is effectively refined by dynamic recrystallization process (DRX) [16]. From **Figure 10**, it was observed that two-pass pressing through die A and die B exhibited bimodal grain structure and more fine grains appeared for the processing in the 90° die than the 110° die. The effectiveness of the grain refinement was observed after four passes of pressing in the 90° die as shown in **Figure 10(b)**. Also, it is noticed that with the increase in the number of ECAP passes, the amount of fine grains is increased greatly.

### 3.1.3 Variation of grain size with two different die after 2 and 4 ECAP passes for AZ80/91 Mg alloys

**Figure 11** displays the variation of average grain size of processed and unprocessed AZ80 and AZ91 Mg alloys of 2 and 4 ECAP passes through die A and die B. As it could be observed from **Figures 6** and **9** as-received and homogenized (OP) Mg alloy has moderately large grain size approximately ~50.20 μm and ~50.70 μm for AZ80 and 58.69 μm, 59.82 μm for AZ91 alloy respectively. The increased average grain size of Mg alloy after homogenization treatment AZ80/91 Mg alloy at 673 K-24 h is due to the phenomenon of grain growth effect [8, 17, 18]. Further, it can be shown that after 2P and 4P ECAP volume fraction of grains increases compared to as-received and homogenized Mg alloy. Mean grain size of AZ80 Mg alloy after ECAP-2P and 4P were ~28.87 μm and ~6.35 μm respectively for die A. Similarly, the average grain size of same Mg alloy processed through die B is ~36.14 μm and ~9.77 μm for ECAP-2P and 4P respectively. Further, an average grain size of AZ91 Mg alloy after 2P and 4P of ECAP were ~30.86 μm, ~7.58 μm for die A and ~36.14 μm, ~9.7 μm for die B respectively. It is apparent that the obtained grain refinement is due to DRX during ECAP and they increase in many ECAP passes which result in much smaller grain structure. However, from this it is noticed that the alloy processed with 90° die shows smaller grain sizes than 110° die for both alloy, this is due to

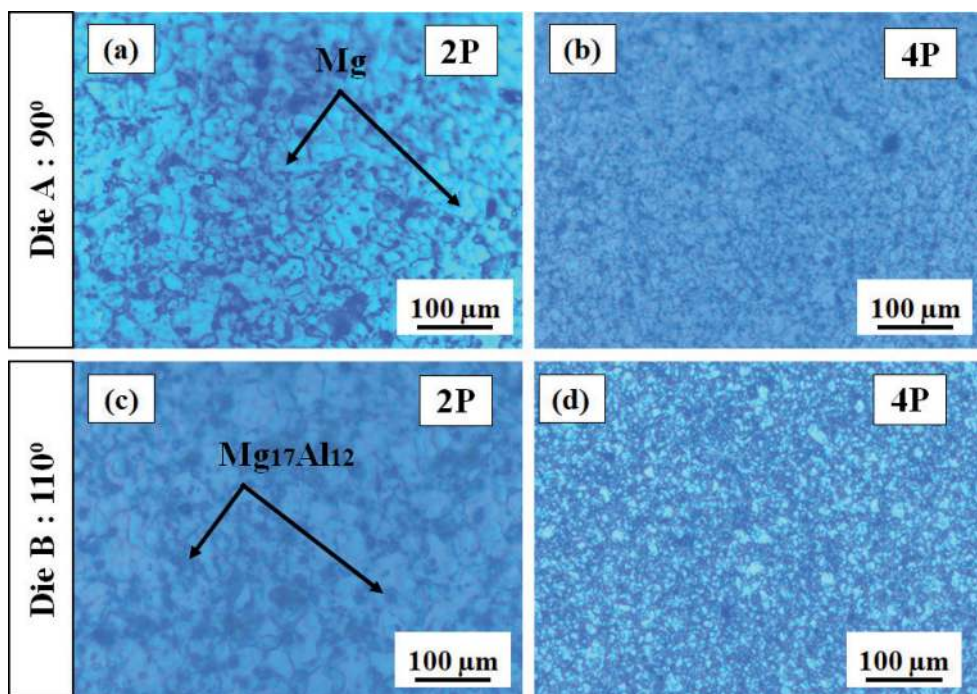


**Figure 10.** Optical images for die A: (a) 2P (b) 4P and die B: (c) 2P and (d) 4P ECAP passes.

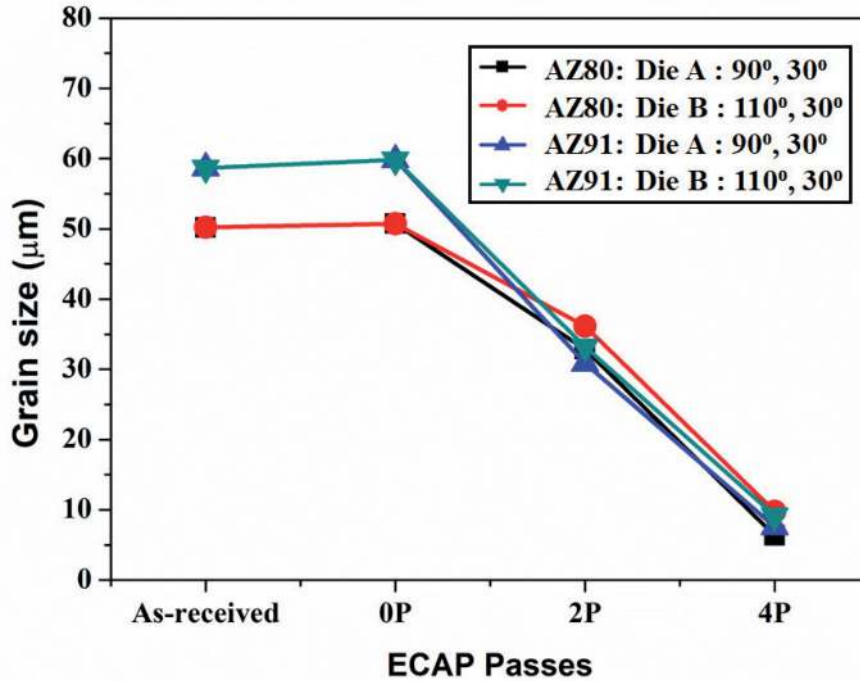


**Figure 11.**  
Variation of average grain size with two different die.

the accumulation of very large plastic strain while processing with a low angle die [19, 20]. The calculated equivalent plastic strain for  $110^\circ$  to be  $\sim 0.742$  and  $\sim 1.015$  for  $90^\circ$  indeed, the strain developed by 4P ECAP through  $90^\circ$  die is higher than that of  $110^\circ$  die. Therefore, large strain in the material exhibited more dislocation density lead to the formation of fine grains during this process. Therefore, undoubtedly it is evident that ECAP die angles significantly affect the deformation homogeneity and this influences the variation in microstructure [21–23].

Also, the microstructural change contributes towards improved mechanical properties and corrosion resistance. Finally, in general, AZ Mg alloy processed through die A and die B showed the same trend of decreasing grain size from the homogenized condition. By extruding in the die A, the mean grain size of AZ80 and AZ91 Mg alloy decreased by 35% and 22% when compared with material processed through die B [19, 20]. Also, from the result, it was observed that AZ80 Mg alloy processed through die A at 598 K exhibited fine grain structure of about  $\sim 6.35 \mu\text{m}$  after four ECAP passes, which is lower when compared to ECAPed AZ91 Mg alloy processed at same processing temperature.

### 3.2 X-ray diffraction analysis

The X-ray diffraction patterns of AZ80/91 Mg alloy before and after ECAP processes as shown in **Figure 8**. The XRD patterns of the as-received, homogenized at 673 K and ECAPed AZ Mg alloys revealed two sets of peaks, one for the  $\alpha$ -Mg primary phase and another one for the  $\beta$ - $\text{Mg}_{17}\text{Al}_{12}$  secondary phase. But as-received alloy of AZ80 has shown new peaks corresponding to the formation of the ternary phase appeared at  $41.4^\circ$  as shown in **Figure 8(a)** which is disappeared after homogenization treatment and ECAP depicts in **Figure 8(b)–(d)** due to diffusion annealing treatment and dynamic precipitation during the ECAP process. Further, **Figure 8(c)** and **(d)** presents the XRD patterns for ECAPed AZ80 Mg alloys for 2P and 4P processed with

die A at processing temperature 598 K. It was observed that the peak intensities were increased after 4P ECAP when compared to the ECAP-2P sample. This is due to an increased volume fraction of secondary phases and more homogenous microstructure. But 2P ECAP processed sample presented lower peak intensity this is mainly due to non-homogeneity in the microstructure and crystal defects.

Furthermore, **Figure 8(e)–(h)** shows the XRD spectra of AZ91 Mg alloy (e) as-received (f) the homogenized at 673 K for 24 h (g) the two-passed AZ91 Mg alloy ECAPed with die A at 598 K and (h) the four-passed AZ91 Mg alloy ECAPed with die A at 598 K. Regardless of the number of ECAP pass, the as-received and processed samples contained  $\alpha$ -Mg and  $\beta$ -Mg<sub>17</sub>Al<sub>12</sub> phase. The intensity of the peak in the ECAP processed specimens at 598 K is lower than that of the as-received specimen. Also, it can be seen that there exists great difference on the magnitude of the peak intensity of ECAP processed specimen at 598 K for two and four passes this is mainly due to induced plastic strain during ECAP similar results has been observed by Avvari et al. [24–28].

### 3.3 Mechanical behavior

This section explains the effect of ECAP die channel angle on mechanical properties of as-received and ECAPed AZ80/91 Mg alloys.

#### 3.3.1 Effect of die parameters and processing temperature on microhardness

**Figure 12** shows the impact of channel angle on microhardness during ECAP of AZ80/91 Mg alloys. From the results, it was observed that AZ80/91 Mg alloy processed through lower channel angle of 90° (die A) exhibited enhanced microhardness when compared to material processed through die B at 598 K after 4 Passes of ECAP. The improved microhardness is mainly due to the accumulation of large plastic strain while processing at 90° channel angle and obtained more equiaxed microstructure.

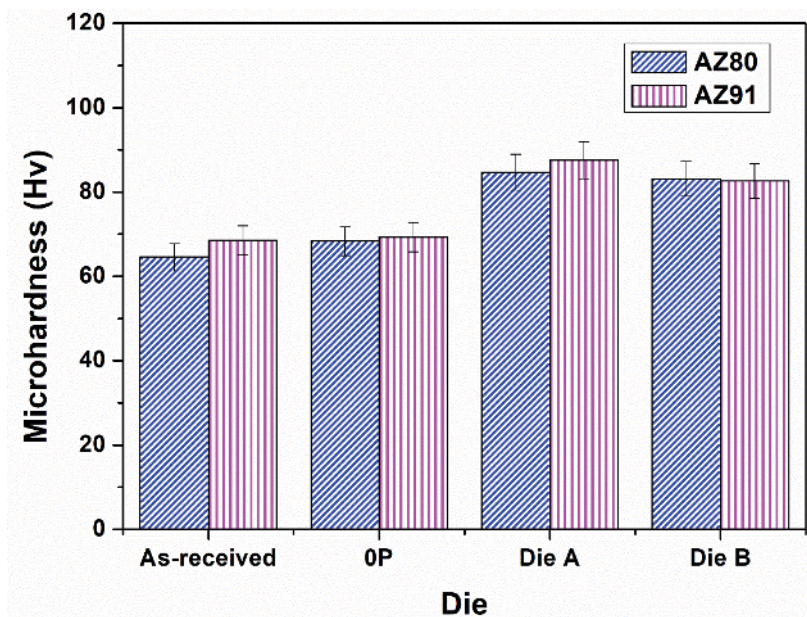


**Figure 12.** Variation of microhardness for AZ80/91 Mg alloys after processing through two different dies.

Hence, die A which has 90° channel angle is considered as an optimal die parameter to get the highest Microhardness for both AZ80/91 Mg alloys. Also, from **Figure 12** it was established that there is a significant increase in Microhardness after a four pass of ECAP in AZ91 Mg alloy after processing using a die A compared to AZ80 Mg alloy processed through the same die and this is anticipated from measurements of the effective refinement of grain size.

### 3.3.2 Variation of tensile strength with two different die and processing temperature

The engineering stress-strain curves of un-ECAPed and ECAPed AZ80/91 Mg alloys at two different dies are shown in **Figure 13**. The stress-strain curves show that ultimate tensile strength and ductility of ECAP-4P processed AZ80 specimens at 598 K are about 489.17 MPa, and 19.03%, respectively for die A, Along with this, the same material processed through die B 4P-ECAP exhibited UTS and %elongation is 451.01 MPa and 11.76% respectively, which are higher than that of an as-received and homogenized specimen of AZ80 Mg alloys. Similarly, the AZ91 Mg alloy processed through die A has greatly improved ultimate tensile strength and ductility. Particularly, as-received AZ91 alloys have 372.74 MPa and 7.84% of UTS and ductility respectively, which is further enhanced to 432.81 MPa and 19.13% after processing through die A for 4 passes and 410.35 MPa and 13.22% of ultimate tensile strength and ductility was observed after processing through die B for 4 passes. From this result, it was found that compared with the ECAPed AZ91 Mg alloys processed with die A, the AZ80 Mg alloy processed through die A exhibited enhanced tensile properties compared to die B. This is due to an induced large amount of plastic strain during ECAP.

### 3.4 Corrosion study

This section illustrates the effect of ECAP die channel angle on corrosion behavior of as-received and ECAPed AZ80/91 Mg alloys. Also, presents the morphology study on corroded surfaces of as-received and ECAPed AZ80/91 Mg alloys.

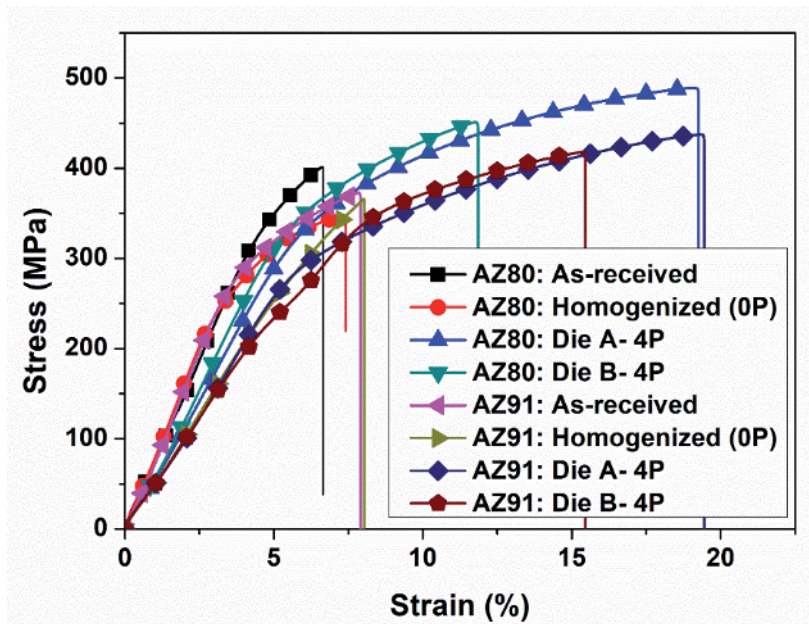


**Figure 13.**  
Variation of tensile strength for different ECAP die.

### 3.4.1 Effect of ECAP die and processing temperature on corrosion rate

The corrosion results of AZ80/91 Mg alloy processed through die A and die B at 598 K after 4-ECAP passes including as-received and homogenized samples were shown in **Figure 14**.

From **Figure 14**, it was observed that the channel angle of ECAP significantly influences the grain refinement and distribution of secondary phases which contribute towards corrosion resistance. ECAP processing through die A at 598 K leads to lower corrosion rate after 4 passes of ECAP compared to die B under the same conditions for both AZ80/91 Mg alloys. This is mainly due to the lower dislocation density at recrystallization temperature [29]. Therefore the reduction of the grain size and the increase of the distribution of secondary phases can cause an improved corrosion resistance. In other words, the column chart shows the variation of corrosion rates of Mg alloys before and after ECAP process for both AZ80/91 Mg alloys. The more ECAP passes are related to the nobler corrosion potentials and the lower current density. The Mg alloy processed through die A and die B after four ECAP passes results that the ECAPed Mg processed through die A has nobler  $E_{\text{corr}}$  and  $I_{\text{corr}}$  values, leads to more corrosion resistance than the specimen extruded through die B, as-received and homogenized. Specifically, AZ91 Mg alloy processed through ECAP after 4 passes exhibited improved corrosion resistance than the ECAPed AZ80 Mg alloys this mainly due to elemental composition of AZ91 Mg alloy.

### 3.4.2 Effect of grain size and distribution of secondary phases on corrosion behavior

**Figure 15** depicts the polarization plots for AZ80 and AZ91 Mg alloys processed with die A at 598 K. From **Figure 15(a)** it was observed that the anodic branches of the unprocessed and processed AZ80 specimen showing the continuous active dissolution of the metal this indicate that AZ80 Mg alloy exhibit poor passivity [30]. Although,  $E_{\text{corr}}$  values of ECAP processed AZ80 Mg alloys are significantly shifted to the less negative potentials and highly reduced the magnitude of  $I_{\text{corr}}$  after 2 passes.

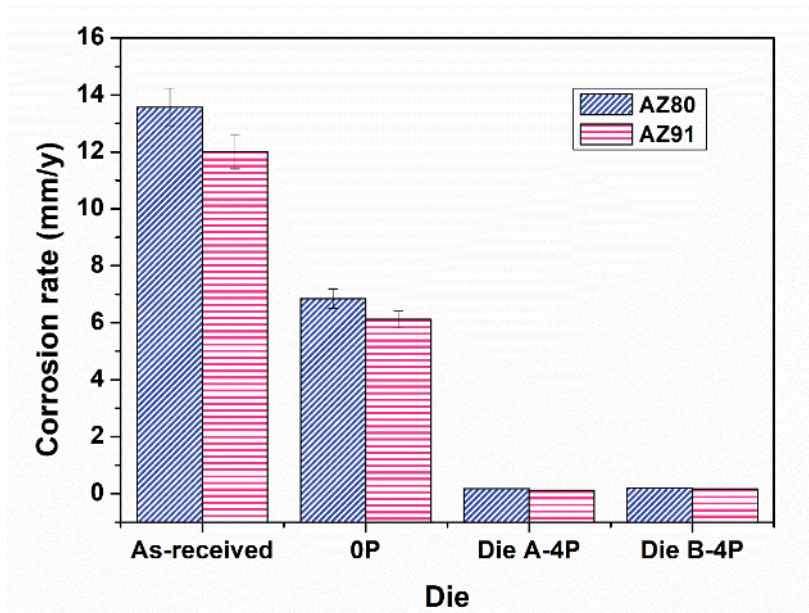


**Figure 14.**  
Corrosion rate vs. ECAP die.

A similar observation was made by Ambat et al. [31]. Further, the polarization plot of the 4P ECAPed with  $90^\circ$  die exhibits a corrosion potential of  $-1.375 V_{SCE}$  this is higher than corrosion potential of other ECAP passes. This indicates that AZ80 Mg alloy processed with  $90^\circ$  die sample has higher pitting corrosion resistance. Moreover, polarization results specify that the ECAPed AZ80 Mg processed with  $90^\circ$  die has nobler  $E_{corr}$  values. Further, the potentiodynamic polarization curves of as-received and ECAPed AZ91 Mg specimens in 3.5 wt.% NaCl was also shown in **Figure 16(b)**. The experimental results revealed that the  $E_{corr}$  corrosion potential of 4P-ECAPed AZ91 Mg alloys was  $-1.453V_{SCE}$ , which was less negative compared with the as-received alloy and other ECAP passes (**Figure 16(b)**). This phenomenon specifies that the cathodic reaction was more difficult in fine-grained Mg alloys compared to the coarse grain alloy. Therefore, with the ECAP, the corrosion potential

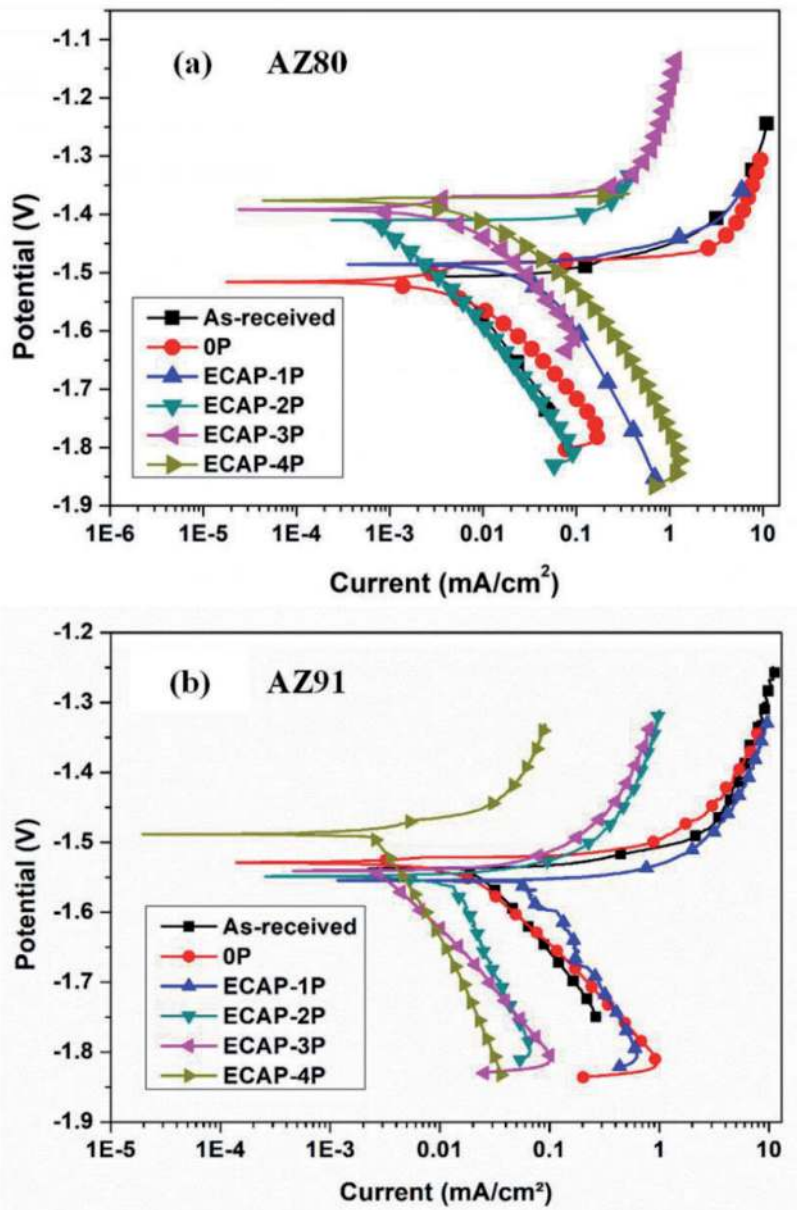


**Figure 15.** Polarization curves of Mg alloys processed through die A (a) ECAPed AZ80 Mg alloys and (b) ECAPed AZ91 Mg alloys.

( $E_{\text{corr}}$ ) shifted to  $-1.536 V_{\text{SCE}}$  and  $-1.453 V_{\text{SCE}}$  after two and four ECAP passes which are considerably nobler in comparison with the as-received alloy ( $-1.540 V_{\text{SCE}}$ ). However, the corrosion potential increases with the grain refinement after ECAE in the alloy. Also, the corrosion current density ( $I_{\text{corr}}$ ) of 2P and 4P ECAPed AZ91 Mg alloy was  $0.0173 \text{ mA/cm}^2$  and  $0.0053 \text{ mA/cm}^2$  respectively, which is lesser than that of as-received AZ91 Mg alloy ( $0.0263 \text{ mA/cm}^2$ ). The obtained results revealed that the ECAPed Mg sample after 4 passes has nobler corrosion potential and lower current density when compared with as-received and ECAPed-2P. Therefore, ECAE increased the corrosion resistance of Mg alloy this is due to grain refinement and distribution of secondary phases, which is shown in OM and SEM microstructure in **Figure 16**. Similarly, Shahar et al. [32] explored that the grain refinement and secondary phase distribution through ECAP improves the corrosion resistance of Mg alloys.

### 3.5 Corrosion morphology

The corrosion morphologies of as-received and as-processed specimens of AZ80 and AZ91 Mg alloys immersed in 3.5 wt.% NaCl solution observed through scanning electron microscopy and is shown in **Figures 16** and **17**.

From **Figures 16(a)**, **(b)** and **17(a)**, **(b)**, it was observed the adequate amount of corrosion attack on the surface of the as-received and homogenized AZ80 and AZ91 Mg alloys after potentiodynamic polarization test. The ECAP performed samples of Mg alloys after the corrosion test exhibited comparatively less localized pits on the surface of ECAPed AZ80/91 Mg alloys have shown in **Figures 16(c)** and **17(c)**. This obtained result showed that pitting corrosion resistance of ECAPed Mg alloys are significantly improved through grain refinement and this is due to the distribution of secondary phases [33–35]. It is worth to declare that this appeared improved for AZ80/91 Mg alloy was due to the grain refinement, distribution of secondary phases and formation of

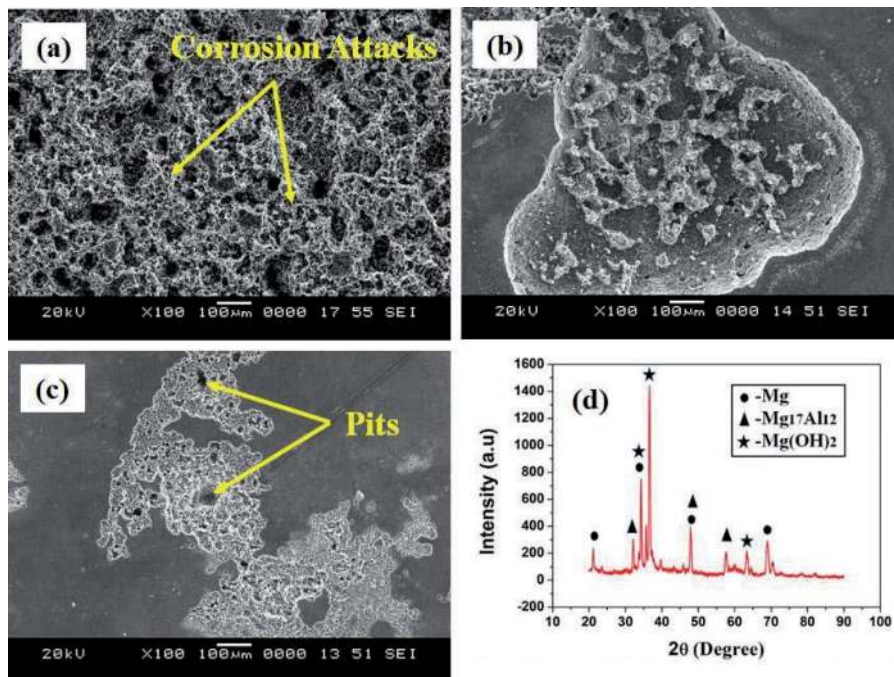


**Figure 16.** Corrosion morphology of AZ80 Mg alloys (a) as-received (b) homogenized at 673 K-24 h (c) 4P-598 K and (d) XRD for a corroded specimen of as-received.

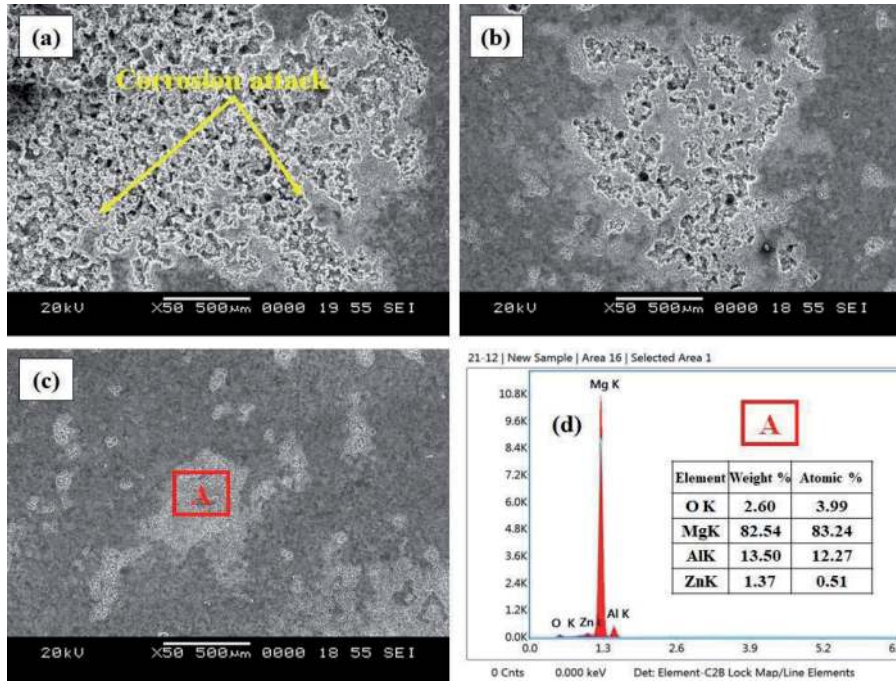


**Figure 17.** Corrosion morphology of AZ91 Mg alloys (a) as-received (b) homogenized at 673 K-24 h (c) 4P-598 K and (d) EDX for corroded ECAP-4P specimen.

magnesium hydroxides formed on their surfaces which proved through microstructure and X-ray diffraction analysis shown in **Figures 16(d)** and **17(d)** for AZ80 and AZ91 Mg alloys respectively. The existence of such metal oxide partially protects the Mg surface from further dissolutions under this circumstance the breakdown of the film and the consequential nucleation and growth of a pit become more difficult. Moreover, the higher  $E_{\text{corr}}$  value for ECAPed Mg alloys at higher passes revealed that the surface of Mg alloys was more passivated against corrosion this is due to slow dissolution rate of fine grains structure [30, 31]. Finally, from the results, it was concluded that the severe corrosion attack was observed on as-received AZ80 and AZ91 Mg alloys and further continuous reduction in corrosion attack was observed for ECAPed samples. Similar kind of results and trends is reported by many authors in their studies [29, 36, 37].

#### 4. Conclusion

AZ80/91 Mg alloy processed through both die A and die B at 598 K were discussed in this chapter. Indeed, Mg alloy processed through die A has significantly shown fine grains than die B. Since the grain size and distribution of secondary phases are a major factor in determining the strength and corrosion resistance of the material respectively, therefore die A is considered as optimal to achieve fine grain structure in our work. As a result, the fine grains obtained through die A exhibited improved mechanical and corrosion resistance discussed in the earlier sections. Also, based on the experimental results and discussion, the following conclusions were drawn.

- Increase in ECAP passes lead to homogeneous microstructure due to dynamic recrystallization which occurred during ECAP process. The secondary  $\beta$ -Mg<sub>17</sub>Al<sub>12</sub> phase was reduced and uniformly distributed throughout the



extruded material. Here, the effectiveness of ECAP with die A in grain refining of AZ80/91 Mg alloys was quite significant because of imposing large plastic strain of ~5.06 after four ECAP passes.

- The average grain size of AZ80 and AZ91 Mg alloy was found to be reduced to 6.35  $\mu\text{m}$  and 7.58  $\mu\text{m}$  respectively after processing through die A at 598 K.
- Microhardness, ultimate tensile strength and ductility for both AZ80 and AZ91 Mg alloy has been enhanced by refining grain size with an increasing number of passes. Ultimate tensile strength of the AZ91 Mg alloy decreased when compared to AZ80 Mg alloy after ECAP this is due to the presence of the secondary  $\beta$ -Mg<sub>17</sub>Al<sub>12</sub> phase.
- Mechanical properties such as ultimate tensile strength, ductility and microhardness of the AZ80/91 Mg alloy are directly proportional to the ECAE passes.
- Potentiodynamic polarization test showed reduced corrosion current density ( $I_{\text{corr}}$ ) which indicates higher corrosion resistance for the ECAP processed samples due to the presence of equiaxed fine grain microstructure and homogeneously distributed secondary particles (Mg<sub>17</sub>Al<sub>12</sub>).
- Polarization results showed that passive behavior of ECAPed AZ80/91 Mg sample enhances compared to as-received AZ80/91 Mg alloy owing to the grain refinement and distribution of secondary phase. An AZ80/91 Mg alloy processed with die A (90°) showed higher pitting corrosion resistance compared to die B (110°), by showing less negative pitting potential during 4P-ECAP. Also, the obtained polarization data have good agreement with the corrosion surface morphology.

## **Author details**

Gajanan Manjunath Naik<sup>1</sup>, Sachin Bandadka<sup>2</sup>, Manjaiah Mallaiah<sup>3\*</sup>,  
Ravindra Ishwar Badiger<sup>4</sup> and Narendranath Sannayellappa<sup>5</sup>

1 Department of Mechanical Engineering, Mangalore Institute of Technology and Engineering, Moodbidri, Mangalore, Karnataka, India

2 Department of Mechanical Engineering, Nitte Meenakshi Institute of Technology, Yelahanka, Bangalore, Karnataka, India

3 Department of Mechanical Engineering, National Institute of Technology Warangal, Telangana, India


4 Department of Mechanical Engineering, Yenepoya Institute of Technology, Moodbidri, Mangalore, Karnataka, India

5 Department of Mechanical Engineering, National Institute of Technology Karnataka, Surathkal, Mangalore, Karnataka, India

\*Address all correspondence to: manjaiahgalpuji@gmail.com

## **IntechOpen**

---

© 2020 The Author(s). Licensee IntechOpen. This chapter is distributed under the terms of the Creative Commons Attribution License (<http://creativecommons.org/licenses/by/3.0>), which permits unrestricted use, distribution, and reproduction in any medium, provided the original work is properly cited. 

## References

- [1] Zhongyu Cui, Xiaogang Li, Kui Xiao, Chaofang Dong. (2013). "Atmospheric corrosion of field-exposed AZ31 magnesium in a tropical marine environment," *Corr. Sci.*, 76, 243-256.
- [2] Noor, E A, A.H. Al-moubaraki. (2008). "Corrosion Behavior of Mild Steel in Hydrochloric Acid Solutions." *Int. J. Electrochem. Sci.*, 3, 806-818.
- [3] Hao-Miao Yang, Nan-Yi Zhang, Na Liu, Wei-Dong Xie, Xiao-Dong Peng. (2016). "Microstructure, mechanical properties, and corrosion resistance of Mg-9Li-3Al-1.6Y alloy." *Rare Metals*, 35, 374-379.
- [4] Bao. L, Z. Zhang, Q. Le, S. Zhang, J. Cui. (2017) "Corrosion behavior and mechanism of Mg-Y-Zn-Zr alloys with various Y/Zn mole ratios," *J. Alloys Comp.*, 712, 15-23.
- [5] Shaeri M.H., Ebrahimi, M.T. Salehi, S.H. Seyyedein. (2016). "Materials International Effect of ECAP temperature on microstructure and mechanical properties of Al – Zn – Mg – Cu alloy." *Prog. Nat. Sci. Mater. Int.*, 26, 182-191.
- [6] Brunner J.G, J. May, H.W. Höppel, M. Göken, S. Virtanen. (2010). "Localized corrosion of ultrafine-grained Al – Mg model alloys." *Electrochimica Acta*, 55, 1966-1970.
- [7] Sun, H. Q., Shi, Y. N., Zhang, M. X., & Lu, K. (2007). "Plastic strain-induced grain refinement in the nanometer scale in a Mg alloy." *Acta Mater.*, 55(3), 975-982.
- [8] Naik, Gajanan M., Gopal D. Gote, S. Narendranath, and SS Satheesh Kumar. (2018). "The impact of homogenization treatment on microstructure microhardness and corrosion behavior of wrought AZ80 magnesium alloys in 3.5 wt% NaCl solution." *Mater. Res. Express*, 5, 086513.
- [9] Naik Gajanan, M, Narendranath, S., & Kumar, S. S. (2019). "Influence of ECAP processing routes on microstructure mechanical properties and corrosion behavior of AZ80 Mg alloy." *AIP Conf. Proc.*, 2082 (1), 030016.
- [10] Naik, G. M., Gote, G. D., & Narendranath, S. (2018). "Microstructural and Hardness evolution of AZ80 alloy after ECAP and post-ECAP processes." *Mater. Today: Proc.*, 5(9), 17763-17768.
- [11] Naik, G. M., Gote, G. D., Narendranath, S., & Kumar, S. S. (2018). "Effect of grain refinement on the performance of AZ80 Mg alloys during wear and corrosion." *Adv. Mater. Res.*, 7(2), 105-118.
- [12] Naik, G. M., Narendranath, S., & Kumar, S. S. (2019). "Effect of ECAP Die Angles on Microstructure Mechanical Properties and Corrosion Behavior of AZ80 Mg Alloy." *J. Mater. Eng. Perform.*, 28(5), 2610-2619.
- [13] Dieter, G. E., & Bacon, D. (1986). "Mechanical metallurgy" (Vol. 3). New York: McGraw-Hill.
- [14] Nagasekhar and Tick-Hon Yip. (2005). "Finite Element Study of Multi pass Equal Channel Angular Extrusion/Pressing." *Int. J. Nanosci.*, 4(4), 745-751.
- [15] Nikulin, I., Kipelova, A., Malopheyev, S., & Kaibyshev, R. (2012). "Effect of second phase particles on grain refinement during equal-channel angular pressing of an Al-Mg-Mn alloy." *Acta Mater.*, 60(2), 487-497.
- [16] Orlov, D., Todaka, Y., Umemoto, M., Beygelzimer, Y., Horita, Z., & Tsuji, N. (2009). "Plastic flow and grain refinement under simple shear-based

- severe plastic deformation processing.” *Mater. Sci. Forum*, 604, 171-178.
- [17] Gajanan, M. N., Narendranath, S., & Kumar, S. S. (2019). “Effect of grain refinement on mechanical and corrosion behavior of AZ91 magnesium alloy processed by ECAE.” *IOP Conf. Series: Mater. Sci. Eng.* 591(1), 012015.
- [18] Naik, G.M., Narendranath, S., Satheesh Kumar, S.S. et al. Effect of Annealing and Aging Treatment on Pitting Corrosion Resistance of Fine-Grained Mg-8%Al-0.5%Zn Alloy. *JOM* 71, 4758-4768 (2019). <https://doi.org/10.1007/s11837-019-03769-1>.
- [19] Agwa, M. A., Ali, M. N., & Al-Shorbagy, A. E. (2016). “Optimum processing parameters for equal channel angular pressing.” *Mech. Mater.*, 100, 1-11.
- [20] Alaneme, K. K., & Okotete, E. A. (2019). “Recrystallization mechanisms and microstructure development in emerging metallic materials: A review.” *J. Sci. Adv. Mater. Devices*, 4(1), 19-33.
- [21] Zhao, X., Li, S., Xue, Y., & Zhang, Z. (2019). “An Investigation on Microstructure, Texture and Mechanical Properties of AZ80 Mg Alloy Processed by Annular Channel Angular Extrusion.” *Mater.*, 12(6), 1001.
- [22] Qiao, J., Zheng, L., Ji, J., Bian, F., He, M., & Niu, T. (2018). “High temperature tensile behavior of Mg-2Al and Mg-6Al alloys.” *Int. J. Mater. Res.*, 109(1), 28-33.
- [23] Kim, W. J., Hong, S. I., Kim, Y. S., Min, S. H., Jeong, H. T., & Lee, J. D. (2003). “Texture development and its effect on mechanical properties of an AZ61 Mg alloy fabricated by equal channel angular pressing.” *Acta Mater.*, 51(11), 3293-3307.
- [24] Avvari, M., & Able, M. (2016). “Microstructure evolution in AZ61 alloy processed by equal channel angular pressing.” *Adv. Mech. Eng.*, 8(6), 1687814016651820.
- [25] Avvari, M., Narendranath, S., & Nayaka, H. S. (2015). “A review on wrought magnesium alloys processed by equal channel angular pressing.” *Int. J. Mater. Prod. Tech.*, 51, 139-164.
- [26] Avvari, M., & Narendranath, S. (2018). “Effect of secondary Mg 17 Al 12 phase on AZ80 alloy processed by equal channel angular pressing (ECAP).” *Silicon*, 10(1), 39-47.
- [27] Avvari, M., & Narendranath, S. (2014). “Influence of Route-R on wrought magnesium AZ61 alloy mechanical properties through equal channel angular pressing.” *J. Magnes. Alloys*, 2(2), 159-164.
- [28] Avvari, M., Narendranath, S., & Nayaka, H. S. (2014). “Effect of Processing Routes on AZ31 Alloy Processed By Severe Plastic Deformation.” *Proc. Mater. Sci.*, 5, 1560-1566.
- [29] Yunchang, Tao Hu, and Paul K. Chu. (2010). “Influence of test solutions on in vitro studies of biomedical magnesium alloys.” *J. Electrochemical Society*, 157 (7), 238-243.
- [30] Wenming, T. I. A. N., Songmei, L. I., Jianhua, L. I. U., Mei, Y. U., & Yujie, D. U. (2017). “Preparation of bimodal grain size 7075 aviation aluminum alloys and their corrosion properties.” *Chinese J. Aero.*, 30(5), 1777-1788.
- [31] Ambat, R., Aung, N. N., & Zhou, W. (2000). “Studies on the influence of chloride ion and pH on the corrosion and electrochemical behaviour of AZ91D magnesium alloy.” *J. Appl. Electroch.*, 30(7), 865-874.
- [32] Shahar, I. A., Hosaka, T., Yoshihara, S., & Macdonald, B. J. (2017). “Mechanical and Corrosion Properties of AZ31 Mg Alloy Processed by

Equal-Channel Angular Pressing and Aging.” *Proc. Eng.*, 184, 423-431.

[33] Gopi, K. R., Nayaka, H. S., & Sahu, S. (2016). “Investigation of microstructure and mechanical properties of ECAP-processed AM series magnesium alloy.” *JMEP*, 25(9), 3737-3745.

[34] Lunder, O., Lein, J. E., Hesjevik, S. M., Aune, T. K., & Nişancioğlu, K. (1994). “Corrosion morphologies on magnesium alloy AZ 91.” *Mater. Corr.*, 45(6), 331-340.

[35] Singh, I. B., Singh, M., & Das, S. (2015). “A comparative corrosion behavior of Mg, AZ31 and AZ91 alloys in 3.5% NaCl solution.” *J. Magnes. Alloys*, 3(2), 142-148.

[36] Zeng, Rong-chang, Jin Zhang, Weijiu Huang, W. Dietzel, K. U. Kainer, C. Blawert, and K. E. Wei. (2006). “Review of studies on corrosion of magnesium alloys.” *Trans. Nonferrous Met. Soc. China*, 16, 763-771.

[37] Cheng, Y. L., Qin, T. W., Wang, H. M., & Zhang, Z. (2009). “Comparison of corrosion behaviors of AZ31, AZ91, AM60 and ZK60 magnesium alloys.” *Trans. nonferrous met. Soc. China*, 19(3), 517-524.